Indonesian Journal of Electrical Engineering and Computer Science
Vol. 41, No. 2, February 2026, pp. 456~469
ISSN: 2502-4752, DOI: 10.11591/ijeecs.v41.i2.pp456-469

Control of multi-level NPC inverters in PV/grid systems using ADRC and MADRC

Gherici Dinar[1], Ahmed Tahour[2]
[1]LSTE Laboratory of Environmental Science and Technology, University Mustapha Stambouli of Mascara, Mascara, Algeria
[2]Ecole Supérieure en Sciences Appliqués ESSA, Tlemcen, Algeria

Article Info

Article history:

Received Oct 2, 2025
Revised Dec 30, 2025
Accepted Jan 11, 2026

Keywords:

Active disturbance rejection controller
Grid
Modified active disturbance rejection controller
Multilevel
Neutral point clamped inverter
Photovoltaic
Total harmonic distortion

ABSTRACT

Grid-connected photovoltaic (PV) systems consist of solar panels that convert sunlight into electrical energy, interconnected directly with the utility grid. These systems comprise several key components: PV, multilevel, controllers, and grid interface equipment. In this context, five-level inverters are increasingly favoured over three-level inverters due to their ability to reduce total harmonic distortion (THD), improve efficiency, and ensure better power quality in grid-connected applications. This research presents a three-level enhanced control scheme aimed at optimizing the performance of a grid-connected photovoltaic system with a five-level inverter. A fractional-order proportional-integral (FOPI) controller is utilized for maximum power point tracking (MPPT) to ensure precise tracking under variable irradiance conditions. At the grid-interface stage, a modified active disturbance rejection controller (MADRC) is developed for grid-interface, featuring an inner loop for DC-link voltage regulation based on Lyapunov theory, leading to improved dynamic performance with lower THD of the grid current and enhanced efficiency. Simulation results highlight the effectiveness of the proposed system. Compared with the FOPI-ADRC, a three-level configuration (0.38% THD), the proposed FOPI-MADRC with a five-level inverter achieves superior performance, with only (0.22% THD). These results confirm the advantages of combining advanced control strategies with multilevel inverter technology in improving both power quality and system efficiency.

Corresponding Author:

Gherici Dinar
LSTE Laboratory of Environmental Science and Technology, University Mustapha Stambouli of Mascara
Mascara, Algeria
Email: dnr.ghrc@gmail.com

1. INTRODUCTION

Energy production is a major challenge for the coming years [1]. Indeed, the energy needs of industrialized societies continue to increase. Solar energy systems production is a major challenge for the coming years, as they are efficient in generating electricity in a clean manner. Solar energy is the most promising renewable energy source, and photovoltaic (PV) power generation has become one of the most used renewable energy power generation methods [2], [3]. The development and utilization of PV power generation technology has received widespread attention in countries all over the world [4], [5].

PV is a process of converting light energy into electrical energy [6], [7]. PV power generation has the advantage of environmental factors and has randomness and volatility. Renewable energy sources, especially PV ones, are becoming more and more interesting due to the predicted lack of conventional sources over the coming years.

The PV grid-connected inverter is an important power electronic converter to realize direct current-alternating current (DC-AC) conversion. The PV grid-connected inverter is the interface between the renewable energy power generation systems and the power grid, and it plays a decisive role in grid-connected power generation. The association of the PV station connected to the electricity network is done using a continuous/alternate current converter.

Generally, in the literature, we note that the work deals with the control of simple classic inverters and even those treated by multilevel inverters have been limited to the classic maximum power point tracking (MPPT) control of the chopper that is upstream of the inverter. It is also noted that there is little work done on nonlinear control of multilevel neutral point clamped (NPC) inverters, or that the work is limited to conducting simulations or carrying out experiments for one type of inverter without comparisons or testing of parameter changes [8]. During the research, no comparison was made with another technology or even with an inverter of another type. This research will mainly focus on controlling the grid-side inverter in order to reduce the harmonic distortion content. The work aims to compare the performance of a three-level and a five-level NPC converter used in a PV generation system connected to a nonlinear electrical network.

The ADRC control strategy is based on the extended state observer (ESO), which constitutes its core and allows estimation and cancellation of various external and internal disturbances of the system in real time [9]. This observer has the advantage that it does not require complete knowledge and exact system control. Furthermore, it allows for reducing the time required to establish a detailed model of the studied system.

The modified active disturbance rejection control (MADRC) refers to various alterations or enhancements made to the standard ADRC design to improve its performance, address specific challenges, or simplify implementation. These modifications often involve changes to the ESO or the feedback control law. The research will also provide a comparison between the performance of ADRC and MADRC controllers in regulating AC grids. Pending the work, PQ theory was used to determine harmonic currents.

The study [10] analyzed a grid-tied PV system, suggesting a control method for the grid-side converter (GSC) using a three-level diode-clamped multilevel inverter with voltage-orientated control (VOC). The performance was assessed based on inverter and grid current and total harmonic distortion (THD) but did not evaluate the PV system's efficiency. Ali *et al.* [11] described a grid-tied PV system using the perturbation and observation (P&O) MPPT algorithm, with model predictive control (MPC) managing real and reactive power. Results showed the MPC effectively connected the solar system to the grid while the MPPT tracked maximum power. A different study [12] focused on simulating a grid-connected PV system with a three-phase inverter and a boost converter. It introduced an advanced MPPT controller using linear matrix inequality (LMI) to improve efficiency and reduce current THD. It compared multi-level inverters and control techniques, finding the three-level NPC inverter with integral backstepping control superior. The active disturbance rejection controller (ADRC) and improved MADRC were proposed *pour une meilleure stabilité et résilience dans diverses* conditions. The research highlights the need for optimizing control systems for grid-connected PV power systems.

To improve power quality in the grid and enhance energy extraction from solar panels, intelligent nonlinear control systems are needed. This paper suggests a new method that combines a MADRC for grid regulation with fractional proportional-integral (FOPI) controllers for MPPT. The goal is to enhance the performance of five-level inverter-based PV systems.

This paper has been organized in four sections, where the first section was the paper introduction. In the second section, we are interested in the modelling of the entire PV system component, going from the PV cell to the connection with the utility grid. The third section was devoted to the mathematical model of the ADRC and MADRC. The simulation results of the three-phase grid-connected PV system are presented in the fourth section.

2. METHOD

2.1. System description

In this section we are interested in the modelling of the entire PV system component going from the PV cell to the connection with the utility grid. The studied system is shown in Figure 1, and it consists of i) a PV panel system, ii) a DC-DC boost converter and MPPT control, and iii) a three- and five-level type NPC inverter connected to the grid.

2.2. PV cell modeling

To explain the modelling of a PV array, an equivalent electrical circuit of the same is shown in Figure 2. Which consists of a current source and a diode with a series and parallel resistor [13]-[15]. The characteristic equation is given as follows:

$$Isc - Id - \frac{Vd}{Rp} - Ipv = 0 \quad (1)$$

where, PV array current I_{pv} can be presented as,

$$Ipv = Isc - \frac{Vd}{Rp} - Id \quad (2)$$

Reverse saturation current of the diode can be given,

$$Irs = Iscref + \left[e^{\left(\frac{qVoc}{NsKAT}\right)} - 1\right] \quad (3)$$

Module saturation current I_0 can be shown as,

$$Io = Irs[\frac{(\frac{T}{Tref})^3}{AK} e^{qCg} * \left(\frac{1}{Tref} - \frac{1}{T}\right)] \quad (4)$$

Finally, PV current equivalent model shown in Figure 2 equation is given as,

$$Ipv = IscNp - NsIo\left[e^{\frac{qVpv+IpvRs}{NsAKT}} - 1\right]Vpv + \frac{IpvRs}{Rp} \quad (5)$$

Where, Ipv=current of PV model, Id=diode current, Isc=short circuit current, Vd=voltage across diode, Rp=resistance in parallel, Rs= series resistance, Voc=open circuit voltage, Ns=number of series strings, K=Boltzmann constant, T=absolute temperature in Kelvin.

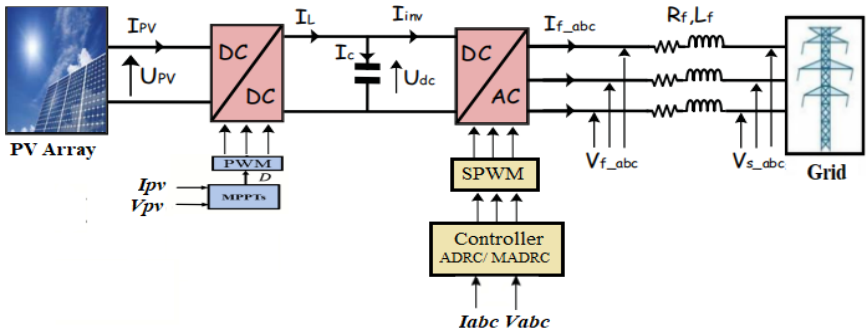

Figure 1. Three phase grid connected PV system

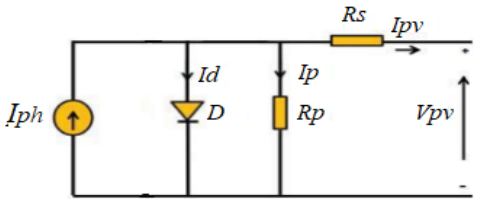

Figure 2. Equivalent model of single diode solar cell

2.3. DC-DC Boost converter and MPPT control

A boost converter increases the value of the input DC voltage to the necessary output voltage level because the DC output voltage of the PV module has a low value that needs to be converted to AC compatible with the grid voltage and frequency. A boost converter is also known as a step-up converter because it uses an inductor, a diode, a capacitor and a high-frequency semiconductor switch to operate [16]-[18]. A DC/DC boost converter is used as a control device due to the wide utilization of such a step-up DC/DC structure in PV systems. Figure 3 shows the corresponding block of a boost converter with load.

$$\frac{dI_L}{dt} = \frac{-(1-D)}{L} V_{out} + \frac{1}{L} V_{in} \quad (6)$$

$$\frac{dV_{out}}{dt} = \frac{(1-D)}{C_{out}} I_L - \frac{1}{RC_{out}} V_{out} \quad (7)$$

Where Vin= input voltage, Vout=output voltage, and D=duty cycle.

Due to their ability to synthesize an output voltage greater than the voltage rating of each switching device, multilevel inverters have several benefits for medium- and high-power systems [19], [20].

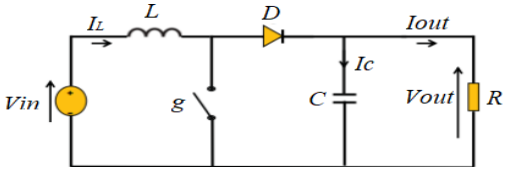

Figure3. DC-DC boost converter model

MPPT is applied in the system to track maximum power output from solar PV. In our work, by combining MPPT with fractional order proportional-integral-derivative (FOPID), we achieve more precise and responsive control of the maximum power point tracking, even under variable conditions such as shading or changing temperature.

FOPID controllers ($PI^{\lambda}D^{\mu}$)are the continuation of conventional PID control, and they are positive real numbers. From the literature, one can also observe that the FOPID controller enhances the system performance, is less sensitive to changes of parameters and attains the property of iso-damping very easily.

The general form of the FOPID controller is defined as [21].

$$C(s)_{FOPID} = \frac{U(s)}{E(s)} = k_P + \frac{k_i}{S^{\lambda}} + k_d S^{\mu} \ (\lambda,\mu \geq 0) \quad (8)$$

Where C(s) is the transfer function model of the FOPID controller, E(s) is an error signal, and U(s) is the controller's output, and the block diagram of the FOPID controller is presented in Figure 4.

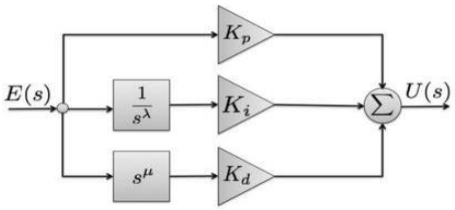

Figure 4. Block diagram FOPID controller

The control signal u(t) is stated in the time domain as,

$$U(t) = k_P + K_i D^{-\lambda} e(t) + k_d D^{\mu} e(t) \quad (9)$$

FOPID-based MPPT offers significant advantages in dynamic performance and robustness for solar systems but demands careful tuning and advanced hardware. It bridges the gap between traditional PID and AI-based methods, making it ideal for applications where efficiency and stability are paramount. For practical implementation, start with simulations (MATLAB) and use metaheuristics for optimization.

3. MULTI-LEVEL CONVERTERS FOR RENEWABLE ENERGY SYSTEMS

Multilevel converters are widely used in renewable energy systems to improve power quality, increase efficiency, and facilitate grid integration. They are particularly beneficial for applications like wind energy systems (WECS) and PV energy systems (PVES), where they can handle variable speeds, eliminate reactive power compensation, and maximize energy extraction. Multilevel inverters are characterized by lower power losses during the switching process [22], [23].

3.1. Description of the NPC topology

The NPC topology is a family of multilevel converters characterized by the use of clamping diodes that divide the voltage across the power switches. The structure of the NPC topology is composed of multiple stages of switches and clamping diodes, arranged to divide the input voltage into multiple output voltage levels. A typical three-level NPC inverter, for example, includes two DC voltage sources, four switches (IGBTs), and two clamping diodes per phase.

The NPC configuration allows for even distribution of voltages and currents between the various switches and diodes, reducing stress on each component. This not only improves component reliability and lifespan but also overall system efficiency. The ability to create multiple intermediate voltage levels also helps to reduce harmonics in the output waveform, thereby improving power quality.

3.1.1. Structure of the three-level NPC

For a three-level NPC topology, the typical structure uses two DC voltage sources (or a DC bus of capacitors). The output voltage is obtained by combining these sources in a controlled manner using the four (4) IGBTs present in the three-level structure. The diodes will be connected between two successive sources, allowing the different intermediate levels to be reproduced. Figure 5 shows the topology of a three-phase, three-level NPC.

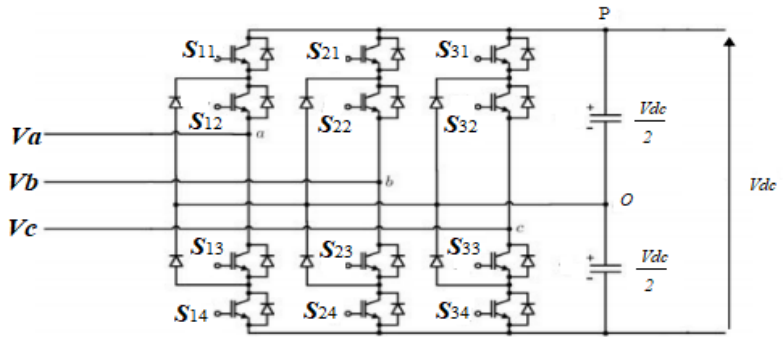

Figure 5. Topology of three-phase three-level NPC

3.1.2. Structure of the five-level NPC

For a five-level NPC topology, the typical structure uses four DC voltage sources (or a DC bus of capacitors). The output voltage is obtained by combining these sources in a controlled manner using the eight (8) IGBTs present in the five-level structure. The diodes will be connected between two successive sources, allowing the different intermediate levels to be reproduced. Figure 6 shows the topology of a three-phase five-level NPC.

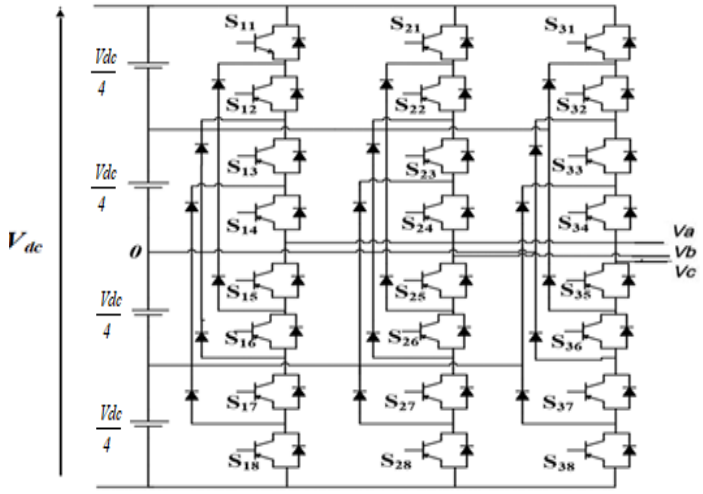

Figure 6. Topology of three-phase five level NPC

4. GRID SIDE CONVERTER MODELING

Electric power generation systems with renewable sources of energy of all kinds, such as wind energy, sea wave energy, solar energy cells, and other various sources, depend on the grid-side converter (GSC), which permits current flow from and to the grid, that main converting DC-link voltage Vdc to AC voltage, or vice versa [24]. Figure 7 depicts the GSC; it consists of 12 electronic switches (S11…S34), and each switch is a phase. A transistor and a diode are connected in parallel, and these twelve switches are distributed over three columns, and the three columns are connected to the grid through three identical coils with L_{filter} inductance and R_{filter} resistance.

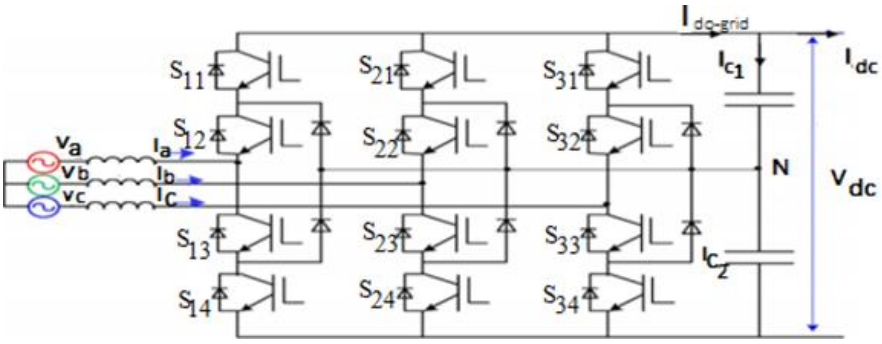

Figure 7. Structure of the grid side converter

A GSC can be represented in a d-q rotating coordinate as follows [25], [26]:

$$\frac{di_d}{dt} = \frac{1}{L_{filter}}(-R_{filter}i_d + \omega_s L_{filter}i_q + V_d - u_d) \quad (10)$$

$$\frac{di_q}{dt} = \frac{1}{L_{filter}}(-R_{filter}i_q - \omega_s L_{filter}i_q + V_q - u_q) \quad (11)$$

The DC link voltage relationship is given as follows [25], [26]:

$$\frac{dV_{dc}}{dt} = \frac{1}{C}(-i_{dc} + i_{dc-grid}) \quad (12)$$

5. LINEAR ADRC CONTROL

Han [27] proposed the effective ADRC technique in 2009 [28]. The tracking differentiator (TD), ESO, and nonlinear state error feedback (NLSEF) are the three primary components of the ADRC controller [24]. Structure of the ADRC controller is illustrated in Figure 8.

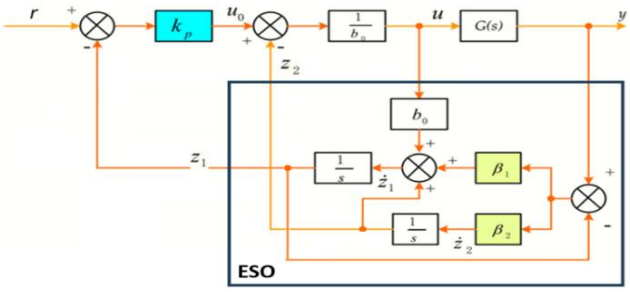

Figure 8. Structure of the ADRC controller

A lot of settings in the ADRC controller need to be changed in practice, and it's difficult to change these parameters [24], [29]. In light of this, a linear ADRC design method is recommended and used to

control the DC link voltage in the grid-side converter, control the speed of the PMSG, and regulate the input current of the boost converter in order to decrease the model complexity and the controller computational requirements.

A proportional controller kp and an ESO make up the LADRC. External disturbances and system uncertainty are seen as a single, generalized disturbance. The generalized disturbance and system states are estimated using the ESO. The tracking error between the system's output and the reference signal is driven to zero by the proportional controller [25], [30].

A first-order system defined by (9) is one with a single input and a single output y.

$$\frac{dy_{(t)}}{dt} = f(y,d,t) + b_0 u_{(t)} \quad (1)$$

Where b_0 is the known portion of the system and *f(y,d,t)* represents the dynamic model and any system disturbances (internal and external). The system described in (9) is given a representation in state variables as shown in (10)-(11).

$$\frac{dz_1}{dt} = z_2 + b_0 u_{(t)} \quad (14)$$

$$\frac{dz_2}{dt} = \frac{df}{dt} \quad (15)$$

The first-order linear ADRC, including the ESO, is given as:

$$\frac{dz_1}{dt} = z_2 + b_0 u_{(t)} - B_1 e \quad (16)$$

$$\frac{dz_2}{dt} = -B_2 e \quad (17)$$

$$e = z_1 - y \quad (18)$$

$$u_{(t)} = \frac{u_o - f}{b_0} \quad (19)$$

$$u_0 = k_p(r - z_1) \quad (20)$$

Where $z_1$is the estimated output. $[B_1 B_2] = [2\omega_0 \omega_0^2]$ it is the observer gain vector. ω_0 Denotes the observer's cut-off pulse; it should be emphasized that while a big pulse allows for a decent assessment of the states, it also runs the danger of making the system more sensitive to noise. It should be observed that a large pulsation allows for the possibility of the estimated variables $z_1 \rightarrow y \; and z_2 \rightarrow f$being used to offset all disturbances by using the control law, as shown in (16).

The controller gain k_p is denoted by ω_c, which is the closed-loop natural frequency, and r is the reference signal. Compared to the dynamics of the controller, the observer's dynamics must be swift. As a result, the observer's poles are positioned to the left of the closed-loop system's poles. Typically, ω_0 is selected so that ω_0= (3-10)k_p [30].

6. VO CONTROL OF GSC

The aim of the control system of GSC is to regulate the DC link voltage at $V_{dc\text{-}ref}$ in the outer loop using ADRC technology and regulate the active and reactive power in the inner loop using a PI controller, where the reference value of the reactive power is equal to zero. Assuming that the coordinate axes (d,q) are orientated so that the d-axis applies to the grid voltage vector V_s, which means V_q=0, then the following two relations can be obtained for the electrical power passed by the GSCs:

$$P = 1.5 V_d i_d = V_{dc-grid} i_{dc-grid} \quad (21)$$

$$Q = -1.5 V_d i_q \quad (22)$$

For a unit power factor, the reference current i_q is set to zero, thus the GSC control system has two regulating axes:

i) q axis: the current i_q is regulated at zero.
ii) d axis: it includes two regulating loops, the first is an external regulating loop through which the DC link voltage is regulated according to the reference value, and the second is an internal regulating loop through which the current i_d is regulated according to the reference value determined by the voltage regulating loop.

7. ADR CONTROL OF DC-LINK VOLTAGE

The implementation of the ADR control is detailed in Figure 9:

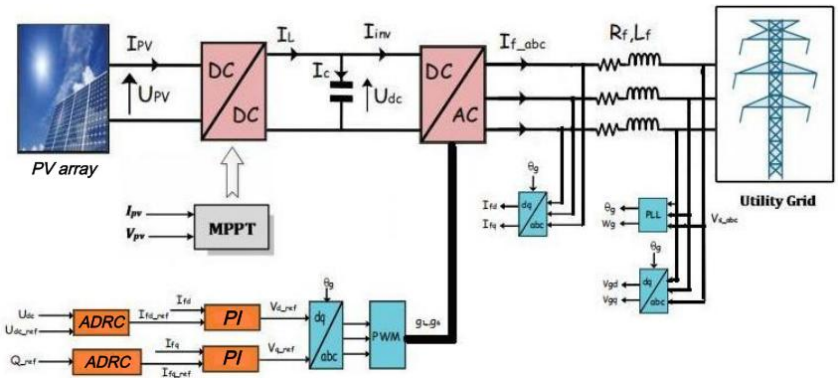

Figure 9. Grid side converter control by ADRC

To control the DC-link voltage, and if we consider that i_q is set to zero, then we can rewrite (8) as follows:

$$\frac{dV_{dc}}{dt} = -\frac{1}{C} i_{dc} + \frac{a}{C} i_d \tag{23}$$

a is related to the transform ratio of GSC.
In (19) can be rewritten as shown:

$$\frac{dV_{dc}}{dt} = f\ (.) + b_0 u \tag{24}$$

The dc-link voltage ADR controller is designed by (22)-(28), as shown:

$$\frac{dz_1}{dt} = f\ (.) + b_o u - B_1 e_1 \tag{25}$$

$$\frac{df\ (.)}{dt} = -B_2 e_1 \tag{26}$$

$$e_1 = z_1 - V_{dc} \tag{27}$$

$$u = \frac{u_o - f\ (.)}{b_o} \tag{28}$$

$$u_o = k_p\ (V_{dc-ref} - z_1) \tag{29}$$

Where:

$$f\ (.) = f(\frac{1}{C} i_{dc}, d) \tag{30}$$

$$b_0 = \frac{a}{C_2} \tag{31}$$

$$u = i_{d-ref} \tag{32}$$

8. MADR CONTROL OF DC-LINK VOLTAGE

A MADRC is a control strategy that builds upon the standard ADRC framework to improve performance and address specific challenges. It often involves modifications to the ESO or the control law itself, aiming for better disturbance rejection, tracking accuracy, or robustness to uncertainties. The grid-side converter control by MADRC is similar to Figure 9, where the ADRC control has been changed to MARDC control.

Neglecting the external disturbance in the relation (19), we find:

$$\frac{dV_{dc}}{dt} = \frac{a}{C_2} i_d \tag{33}$$

Suppose the following error relationship:

$$e_2 = V_{Ref} - k_n V_{dc} \tag{34}$$

By derivation, after substituting the relation (29), we find:

$$\dot{e_2} = -k_n \frac{a}{C_2} i_d \tag{35}$$

Assuming a Lyapunov function:

$$V = 0.5 e_2^2 \tag{36}$$

By deriving the Lyapunov function and substituting the relation (31), we find:

$$\dot{V} = -e_2 k_n \frac{a}{C_2} i_d \tag{37}$$

The control lawi_d can be chosen as follows:

$$i_d = \frac{kC_2}{k_n a} e_2 \tag{38}$$

Compensation in the relationship (33) we find:

$$\dot{V} = -k e_2^2 \tag{39}$$

Therefore, a positive value of k must be chosen to ensure the stability of the system.

Thus, based on the relations (29)-(35), the following differential relation can be written expressing the transfer function between V_{ref} and V_{dc}:

$$\frac{dV_{dc}}{dt} = -kV_{dc} + \frac{k}{k_n} V_{ref} \tag{40}$$

Redesigning the ADRC controller to regulate DC-link voltage based on (36) will be as follows:

$$\frac{dz_1}{dt} = f(.) + b_o V_{ref} - B_1 e_1 \tag{41}$$

$$\frac{df\ (.)}{dt} = -B_2 e_1 \tag{42}$$

$$e_1 = z_1 - V_{dc} \tag{43}$$

$$V_{ref} = \frac{u_o - f(.)}{b_o} \tag{44}$$

$$u_o = k_p\ (V_{dc-ref} - z_1) \tag{45}$$

Where:

$$f(.) = f(-kV_{dc}, d_1) \quad (46)$$

$$b_o = \frac{k}{k_n} \quad (47)$$

$$u = V_{ref} \quad (48)$$

9. RESULTS AND DISCUSSION

The simulation was exacted using MATLAB/Simulink software. Simulations were conducted for using the three-and five-level type (NPC) inverter in the PV/grid. In this section we present the simulation results of the proposed control strategy for a PV system connected to three-phase utility grid (380 v/50 Hz). Simulation were conducted for using the three-and five-level (NPC) inverters of proposed control ADRC and MADRC.

The DC link voltage was maintained to its reference as it is shown in Figure 10, which illustrates the response of different control systems in regulating the DC link voltage. From this figure, a comparison for Vdc between using a three level (NPC) converter and a five level (NPC) converter is reviewed with the applied of two different control techniques ADRC and MADRC control.

The DC-link voltage is plotted over time, with the reference voltage set at 625 V. All four systems start at the same initial voltage and attempt to reach and maintain the reference value. The five-level inverter controlled using MADRC achieves the reference voltage rapidly (625 V within 0.02 to 0.2 seconds) and exhibits minimal oscillations, reflecting its superior stability. The three-level inverter controlled using MADRC shows the second-best performance, with a slightly slower response time and marginally more oscillation than the ADRC. The three-level inverter controlled using ADRC exhibits the slowest response and the most significant oscillations around the reference voltage. Notably, all systems experience some disturbances, likely corresponding to changes in solar radiation, but the MADRC controlled shows superior ability in quickly overcoming these disturbances and returning to the reference voltage. This graph clearly illustrates the enhanced dynamic performance and disturbance rejection capabilities of MADRC control strategies, particularly the five levels using MADRC control, in maintaining a stable DC-link voltage under varying conditions.

The active power transmitted to the grid under different control systems is illustrated in Figure 11. The characteristic shows four distinct curves representing the performance of various control strategies. The blue curve corresponds to the three-level (NPC) inverter with ADRC controller, the red curve corresponds to the five-level (NPC) inverter with ADRC controller, the yellow curve corresponds to the three-level (NPC) inverter with MADRC controller, and the violet curve corresponds to the five-level (NPC) inverter with MADRC controller. This is the fourth control system that achieves the highest active power transmission to the grid, Table 1 for the parameter of the ADRC and MADRC controller.

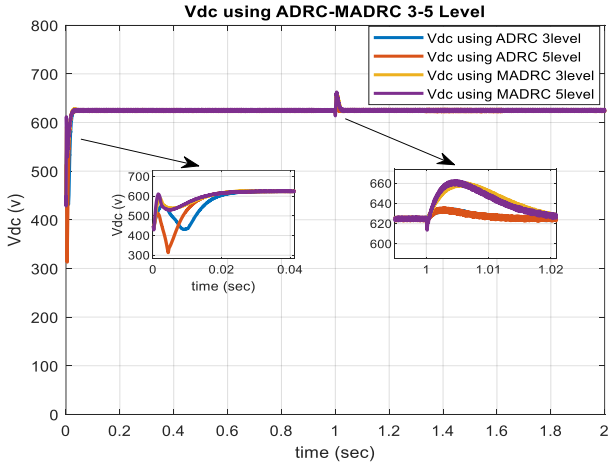

Figure 10. Control systems response to regulate the DC-link voltage

Table 1. The parameter of the ADRC and MADRC controller

Parameters	Lf	Rf	C2	ki	kp	b0
Values	0.6e-3	30*Lf	7000e-6	90	50	1/7000e-6

We note the presence of a transient power peak (during the setpoint change) that is much more significant in the case of three-level inverter controlled using ADRC. This certainly favours five-level inverter controlled using MADRC when we know that these peaks can disrupt the operation of the system or even seriously damage its electronic components. Another parameter for comparison can be observed: the resynchronization time following a change in the reference value of the active power. Here too, the advantage is clearly on the side of MADRC control. In addition, the static error is lower in the case of MADRC control, which results in a better quality output current. The reactive power exchanged with the grid under different control systems is illustrated in Figure 12.

Figure 13 and Table 2 illustrate the THD curve of the current exchanged with the grid under different controls. The results reveal the use of a five-level (NPC) inverter with an MADRC controller. Leads to significantly lower (THD) values compared to three levels (NPC) with an ADRC controller. Demonstrating its effectiveness and efficiency in reducing harmonic distortions and thus enhancing the quality of power transmission. The figure underscores the importance of using advanced control strategies like MADRC with five levels (NPC) to achieve cleaner and more efficient power exchange with the grid, ultimately leading to improved overall system stability and efficiency.

The results of spectral analysis for the grid phase current are illustrated in Figure 14. Show that the five-level (NPC) inverter with the MADRC controller guarantees a better wave quality of the grid current. Grid current FFT analysis using ADRC 3 Level has been illustrated in Figure 14(a); grid current FFT analysis using ADRC 5 Level has been illustrated in Figure 14(b); grid current FFT analysis using MADRC three-level has been illustrated in Figure 14(c); and grid current FFT analysis using MADRC five-level has been illustrated in Figure 14(d).

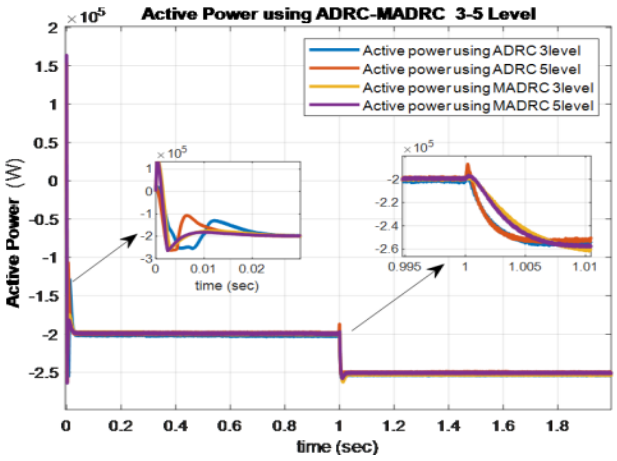

Figure 11. Active power transmitted to the grid

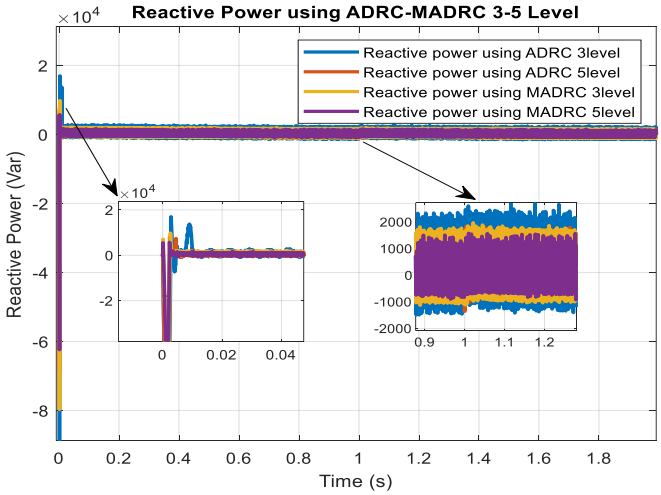

Figure12. Reactive power exchanged with grid

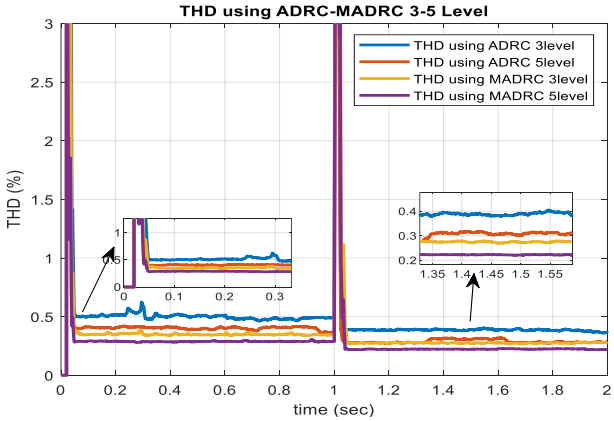

Figure13. THD feature of the current exchanged with the grid

Table 2. THD comparison of three-and five level inverters based ADRC controller and MADRC

Inverter	THD
3 level controlled by ADRC	0.38%
5 level controlled by ADRC	0.28%
3 level controlled by MADRC	0.28%
5 level controlled by MADRC	0.22%

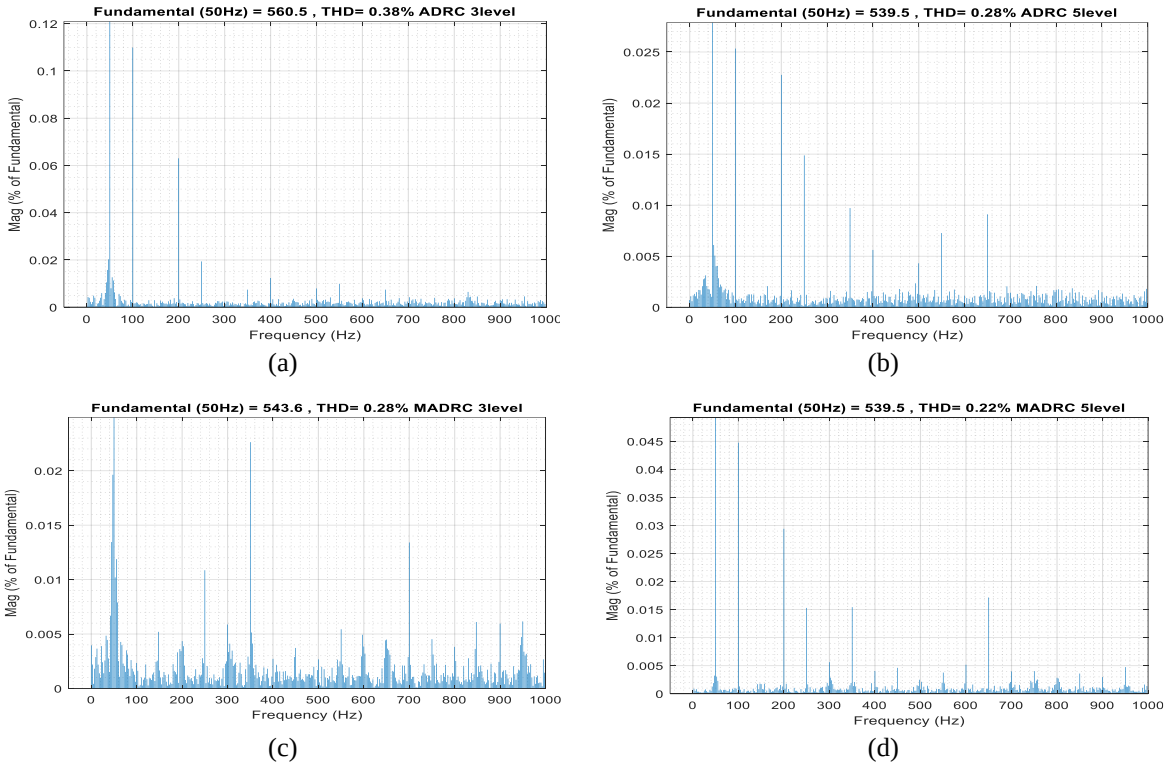

Figure14. Grid current FFT analysis: (a) FFT using ADRC 3 level, (b) FFT using ADRC 5 level, (c) FFT using MADRC 3 level, and (d) FFT using MADRC 5 level

The FFT analysis of the current exchanged with the grid when three-and five-level ADRC and three- and five-level MADRC controllers are employed. The analysis demonstrates a significant reduction in harmonic components across the frequency spectrum, confirming the effectiveness of MADRC control in minimizing distortion. Unlike ADRC-controlled, which exhibits noticeable harmonic peaks, the MADRC-controlled maintains a cleaner current waveform, closer to the ideal sinusoidal shape. This improvement in harmonic suppression is crucial for enhancing the power quality and ensuring stable grid operation.

10. CONCLUSION

The present study assessed the analysis of a grid-connected PV system using a three- and five-level inverter with advanced control strategies. A control methodology employing two stages that combine FOPI MPPT and a MADRC for the grid interface was proposed (FOPI-MADRC).

To confirm the effectiveness of the FOPI-MADRC proposed system, a comparison was made with different configurations, including the FOPI with a three- and five-level inverter controlled by the traditional ADRC, as well as with a configuration including the FOPI controller with an inverter controlled by the MADRC controller in the case of three-level and five-level inverters. The simulation results are then presented for four scenarios: three-level inverter controlled using the ADRC, five-level inverter controlled using the ADRC, three-level inverter controlled using the MADRC, and five-level inverter controlled using the MADRC. It should be noted that PQ theory was used to determine the reference values for the currents in the inner loop in order to reduce the distortion harmonic factor, which was reduced to values ranging from (0.28% to 0.22 %) when the three- and five-level (NPC) inverter was controlled using the MADRC and to values ranging from (0.38% to 0.28 %) when the three- and five-level (NPC) inverter was controlled using the ADRC.

This significant improvement in power quality confirms the advantage of combining multilevel inverter technology with advanced control techniques. Overall, the proposed methodology provides a sustainable optimization of energy harvesting, efficiency, and grid power quality, providing a reliable and efficient solution for grid-connected PV systems and offering a practical path for future large-scale deployments.

FUNDING INFORMATION

Authors state no funding involved.

CONFLICT OF INTEREST STATEMENT

Authors state no conflict of interest.

DATA AVAILABILITY

Data availability is not applicable to this paper as no new data were created or analyzed in this study.

REFERENCES

[1] E. H. M. NDiaye, A. Ndiaye, and M. Faye, "Design and implementation of a hybrid neuro-fuzzy corrector for DC bus voltage regulation," *EAI Endorsed Transactions on Energy Web*, vol. 8, no. 32, p. e15, Oct. 2020, doi: 10.4108/eai.8-10-2020.166551.

[2] H. Hu, S. Harb, N. Kutkut, I. Batarseh, and Z. J. Shen, "A review of power decoupling techniques for microinverters with three different decoupling capacitor locations in PV systems," *IEEE Transactions on Power Electronics*, vol. 28, no. 6, pp. 2711–2726, Jun. 2013, doi: 10.1109/TPEL.2012.2221482.

[3] T. Duman, S. Marti, M. Moonem, A. A. Kader, and H. Krishnaswami, "A modular multilevel converter with power mismatch control for grid-connected photovoltaic systems," *Energies*, vol. 10, no. 5, p. 698, May 2017, doi: 10.3390/en10050698.

[4] R. Siddiqui *et al.*, "Comparison of different technologies for solar PV (photovoltaic) outdoor performance using indoor accelerated aging tests for long term reliability," *Energy*, vol. 107, pp. 550–561, Jul. 2016, doi: 10.1016/j.energy.2016.04.054.

[5] A. K. Tossa *et al.*, "Energy performance of different silicon photovoltaic technologies under hot and harsh climate," *Energy*, vol. 103, pp. 261–270, May 2016, doi: 10.1016/j.energy.2016.02.133.

[6] M. Tivanov, "Calculation of the ultimate efficiency of p-n-junction solar cells taking into account the semiconductor absorption coefficient," *Przegląd Elektrotechniczny*, vol. 1, no. 8, pp. 87–89, 2016, doi: 10.15199/48.2016.08.23.

[7] N. N. Syamimi *et al.*, "Effect of low temperature annealing on anatase TiO2 layer as photoanode for dye-sensitized solar cell," *Przegląd Elektrotechniczny*, vol. 97, no. 10, pp. 12–16, Sep. 2021, doi: 10.15199/48.2021.10.03.

[8] M. Et-Taoussi and H. Ouadi, "Power quality control for grid connected photovoltaic system with neutral point converter," in *2016 International Renewable and Sustainable Energy Conference (IRSEC)*, Nov. 2016, pp. 1040–1045, doi: 10.1109/IRSEC.2016.7983887.

[9] A. J. Laafou, A. A. Madi, A. Addaim, and A. Intidam, "Dynamic modeling and improved control of a grid-connected DFIG used in wind energy conversion systems," *Mathematical Problems in Engineering*, vol. 2020, pp. 1–15, Jul. 2020, doi: 10.1155/2020/1651648.

[10] K. Matiyali, S. K. Goel, and H. Joshi, "Voltage oriented control of grid-tied solar PV system," in *2019 Women Institute of Technology Conference on Electrical and Computer Engineering (WITCON ECE)*, Nov. 2019, pp. 28–34, doi: 10.1109/WITCONECE48374.2019.9092933.

[11] A. I. M. Ali, E. E. M. Mohamed, and A.-R. Youssef, "MPPT algorithm for grid-connected photovoltaic generation systems via model predictive controller," in *2017 Nineteenth International Middle East Power Systems Conference (MEPCON)*, Dec. 2017, pp. 895–900, doi: 10.1109/MEPCON.2017.8301286.

[12] B. Afif, M. Salmi, M. Berka, and U. Özkaya, "Enhancing efficiency and power quality in grid-connected photovoltaic systems based on linear matrix inequality methodology," *Electrical Engineering*, vol. 107, no. 10, pp. 12739–12752, Oct. 2025, doi: 10.1007/s00202-025-03173-w.

[13] H. Can, "Model of a photovoltaic panel emulator in MATLAB-Simulink," *Turkish Journal of Electrical Engineering and Computer Sciences*, Jan. 2013, doi: 10.3906/elk-1105-29.
[14] J. I. Rosell and M. Ibáñez, "Modelling power output in photovoltaic modules for outdoor operating conditions," *Energy Conversion and Management*, vol. 47, no. 15–16, pp. 2424–2430, Sep. 2006, doi: 10.1016/j.enconman.2005.11.004.
[15] A. A. Hocine, T. Mustapha, D. E. Chaouch, and K. Brahim, "An offline trained artificial neural network to predict a photovoltaic panel maximum power point," *Revue Roumaine des Sciences Techniques Serie Electrotechnique et Energetique*, vol. 61, no. 3, pp. 255–257, 2016.
[16] M. L. Frikh, F. Soltani, N. Bensiali, N. Boutasseta, and N. Fergani, "Fractional order PID controller design for wind turbine systems using analytical and computational tuning approaches," *Computers and Electrical Engineering*, vol. 95, p. 107410, Oct. 2021, doi: 10.1016/j.compeleceng.2021.107410.
[17] M. H. Osman, M. A. Elseify, M. K. Ahmed, N. V. Korovkin, and A. Refaat, "Maximum power point tracking for grid-tied PV system using adaptive neuro-fuzzy inference system," in *2021 International Conference on Electrotechnical Complexes and Systems (ICOECS)*, Nov. 2021, pp. 534–540, doi: 10.1109/ICOECS52783.2021.9657445.
[18] B. Wafa, M. Raihane, and B. Hani, "Optimization of fractional order PI controller using meta-heuristics algorithms applied to multilevel inverter for grid-connected PV," *Diagnostyka*, vol. 24, no. 3, pp. 1–10, Sep. 2023, doi: 10.29354/diag/171430.
[19] M. Al-Dhaifallah, "Fuzzy fractional-order PID control for heat exchanger," *Alexandria Engineering Journal*, vol. 63, pp. 11–16, Jan. 2023, doi: 10.1016/j.aej.2022.07.066.
[20] F. Blaabjerg, Z. Chen, and S. B. Kjaer, "Power electronics as efficient interface in dispersed power generation systems," *IEEE Transactions on Power Electronics*, vol. 19, no. 5, pp. 1184–1194, 2004, doi: 10.1109/TPEL.2004.833453.
[21] R. Rajesh, "Optimal tuning of FOPID controller based on PSO algorithm with reference model for a single conical tank system," *SN Applied Sciences*, vol. 1, no. 7, p. 758, Jul. 2019, doi: 10.1007/s42452-019-0754-3.
[22] J. Iwaszkiewicz and P. Mysiak, "Supply system for three-level inverters using multi-pulse rectifiers with coupled reactors," *Energies*, vol. 12, no. 17, p. 3385, Sep. 2019, doi: 10.3390/en12173385.
[23] K. Parfianowicz, "Comparative analysis of multilevel voltage source inverters used to supply a five-phase permanent magnet synchronous motor," *Przegląd Elektrotechniczny*, vol. 98, no. 10, p. 90, Oct. 2022, doi: 10.15199/48.2022.10.17.
[24] I. Aboudrar, S. El Hani, H. Mediouni, A. Aghmad, and M. S. Heyine, "Robust control of three phase grid connected PV system based on ADRC and fuzzy," in *2018 6th International Renewable and Sustainable Energy Conference (IRSEC)*, Dec. 2018, pp. 1–6, doi: 10.1109/IRSEC.2018.8702950.
[25] X. Zhou, J. Wang, and Y. Ma, "Linear active disturbance rejection control of grid-connected photovoltaic inverter based on deviation control principle," *Energies*, vol. 13, no. 15, p. 3790, 2020, doi: 10.3390/en13153790.
[26] F. E. Tahiri, K. Chikh, A. El Afia, J. Lamterkati, and M. Khafallah, "Simulation and experimental validation of VOC and hysteresis control strategies of unit power factor three-phase PWM rectifier," in *2017 International Conference on Electrical and Information Technologies (ICEIT)*, Nov. 2017, pp. 1–6, doi: 10.1109/EITech.2017.8255238.
[27] J. Han, "From PID to active disturbance rejection control," *IEEE Transactions on Industrial Electronics*, vol. 56, no. 3, pp. 900–906, Mar. 2009, doi: 10.1109/TIE.2008.2011621.
[28] H. Aoudjeregba, "A robust controller based on backstepping-ADRC for WRSG based wind turbine," *Przegląd Elektrotechniczny*, vol. 100, no. 3, pp. 176–183, Mar. 2024, doi: 10.15199/48.2024.03.32.
[29] B. Du, S. Wu, S. Han, and S. Cui, "Application of linear active disturbance rejection controller for sensorless control of internal permanent-magnet synchronous motor," *IEEE Transactions on Industrial Electronics*, vol. 63, no. 5, pp. 3019–3027, May 2016, doi: 10.1109/TIE.2016.2518123.
[30] A. J. Laafou, A. A. Madi, Y. Moumani, and A. Addaim, "Proposed robust ADRC control of a DFIG used in wind power production," *Bulletin of Electrical Engineering and Informatics (BEEI)*, vol. 11, no. 3, pp. 1210–1221, Jun. 2022, doi: 10.11591/eei.v11i3.3539.

BIOGRAPHIES OF AUTHORS

Gherici Dinar was born in 1987, is a Ph.D. student at University Mustapha Stambouli of Mascara, Algeria. He used worked in a Portuguese Company EURL EFACEC (electrical network) and now he work in an Electricity Distribution Company (SONELGAZ). With a focus on energy management and optimization methods for the grid within the electrical engineering, non linear control and renewable energy. He can be contacted at email: dnr.ghrc@gmail.com.

Ahmed Tahour was born in 1972 in Ouled Mimoun, Tlemcen, Algeria. He received his BS degree in electrical in 1996, and the MS degree in 1999 and the Ph.D. in 2007 from the Electrical Engineering Institute of the University of Sidi Bel Abbes (Algeria). He is currently Professor of electrical engineering at School Superior of Applied Sciences of Tlemcen (Algeria). He serves as editor in international journals (IJEAEEE) and as a reviewer in RRST, Elsevier (IJEPES, CEP). He serves as a reviewer and international programme committee in international conferences: SEB (2014-2023), ICRERA (2014-2025). His current research interests include power electronics, control of electrical machines and renewable energies. He can be contacted at email: tahourahmed@yahoo.fr.